Hindawi
Geofluids
Volume 2022, Article ID 6416174, 22 pages
https://doi.org/10.1155/2022/6416174

Research Article

Genesis of the Daping Gold Deposit in the Middle Xuefeng Mountain Area, Southern China: Constraints from Geochemistry, Fluid Inclusion, and H-O-S Isotope

Xu Kong,[1,2,3] **Wen-Tian Mi**,[1,4,5,6] **Xue-Yuan Qi**,[4] **Shu-Jun Lǔ**,[3] **Yu-Jun Dong**,[3] **and Jie Xin**[4]

[1]*Key Laboratory of Metallogenic Prediction of Nonferrous Metals and Geological Environment Monitoring (Central South University), Ministry of Education, Changsha 410083, China*
[2]*Department of Geology, Northwest University, Xi'an 710069, China*
[3]*No.407 Geological Team, Hunan Bureau of Geology and Mineral Exploration and Development, Huaihua 418000, China*
[4]*School of Mines, Inner Mongolia University of Technology, Hohhot 010051, China*
[5]*Key Laboratory of Geoscience Spatial Information of Land and Resources, Chengdu 610059, China*
[6]*Geomathematics Key Laboratory of Sichuan Province, Chengdu 610059, China*

Correspondence should be addressed to Xu Kong; konx163@163.com and Wen-Tian Mi; miwentian1982@imut.edu.cn

Received 22 August 2021; Revised 20 September 2021; Accepted 23 September 2021; Published 10 March 2022

Academic Editor: Yong-Zheng Wu

The medium-sized Daping gold deposit is located in the middle Xuefeng Mountain area of Southern China with gold ores hosted in sericite phyllite, sericitolite, and mylonite. The auriferous quartz-carbonate-sulfide veins and adjacent alteration rocks are structurally controlled within the NE (northeast) shear zone with NE, NNE (north-east-east), and NW (northwest) trending at high inclination angles. The petrogeochemistry analysis results show that the gold ores are characterized by high content values of SiO_2, S, and As and low content values of Al_2O_3 and Na_2O and display strong enrichment of LREE with δEu values ranging from 0.54 to 0.75. Four stages of mineralization/alteration were identified: the first stage has mineral assemblages of quartz+pyrite+arsenopyrite±carbonate minerals, the second stage has mineral assemblages of quartz+polymetallic sulfide minerals (pyrite, arsenopyrite, chalcocite, galena, chalcopyrite, tetrahedrite)±chlorite±carbonate minerals, the third stage has mineral assemblages of quartz and carbonate minerals, and the supergene stage is characterized by limonite±patina which were formed by the oxidation of metal sulfides. Among them, the first stage and the second stage are the main gold mineralization stages. The ore-forming fluid inclusions in quartz are mainly composed of liquid phase (H_2O) and gas phase (H_2O and CO_2), and based on the microthermometric analysis, the first metallogenic stage and second metallogenic stage yielded average homogenization temperature of 184.5 and 255.8°C and average salinity of 7.64 wt.% NaCl eqv. and 11.35 wt.% NaCl eqv., respectively. Thus, the ore-forming fluids belong to H_2O-CO_2-NaCl, medium-low temperature, and medium-low salinity fluid. The δD_{H_2O} and $\delta^{18}O_{H_2O}$ values of auriferous quartz are from -51‰ to 62‰ and from -1.44‰ to 5.42‰, respectively, indicating that the ore-forming fluids may belong to mixing fluids of the magmatic fluid and meteoric hydrothermal fluid. The values of $\delta^{34}S$ of metal sulfides range from -0.94‰ to 1.98‰ (-0.131‰ in average), implying that sulfur may source from the concealed granite and/or basement metamorphic strata. The Daping gold deposit formed in the Indosinian period under the tectonic environment of compression between the Cathaysian plate and Yangtze plate and may belong to orogenic gold deposits.

1. Introduction

As one of the crucial gold producers of south China, the Jiangnan Orogen Belt (JOB) has a total gold reserve of >970 tons [1] and thus attracted more and more attention from the metallogeny geologists. The middle Xuefeng Mountain which belongs to the western section of the Jiangnan Orogen is located in the transitional region between the Cathaysia plate and the Yangtze plate (Figure 1(a)) [1–8]. At present, 21 gold deposits (points) have been discovered, and among

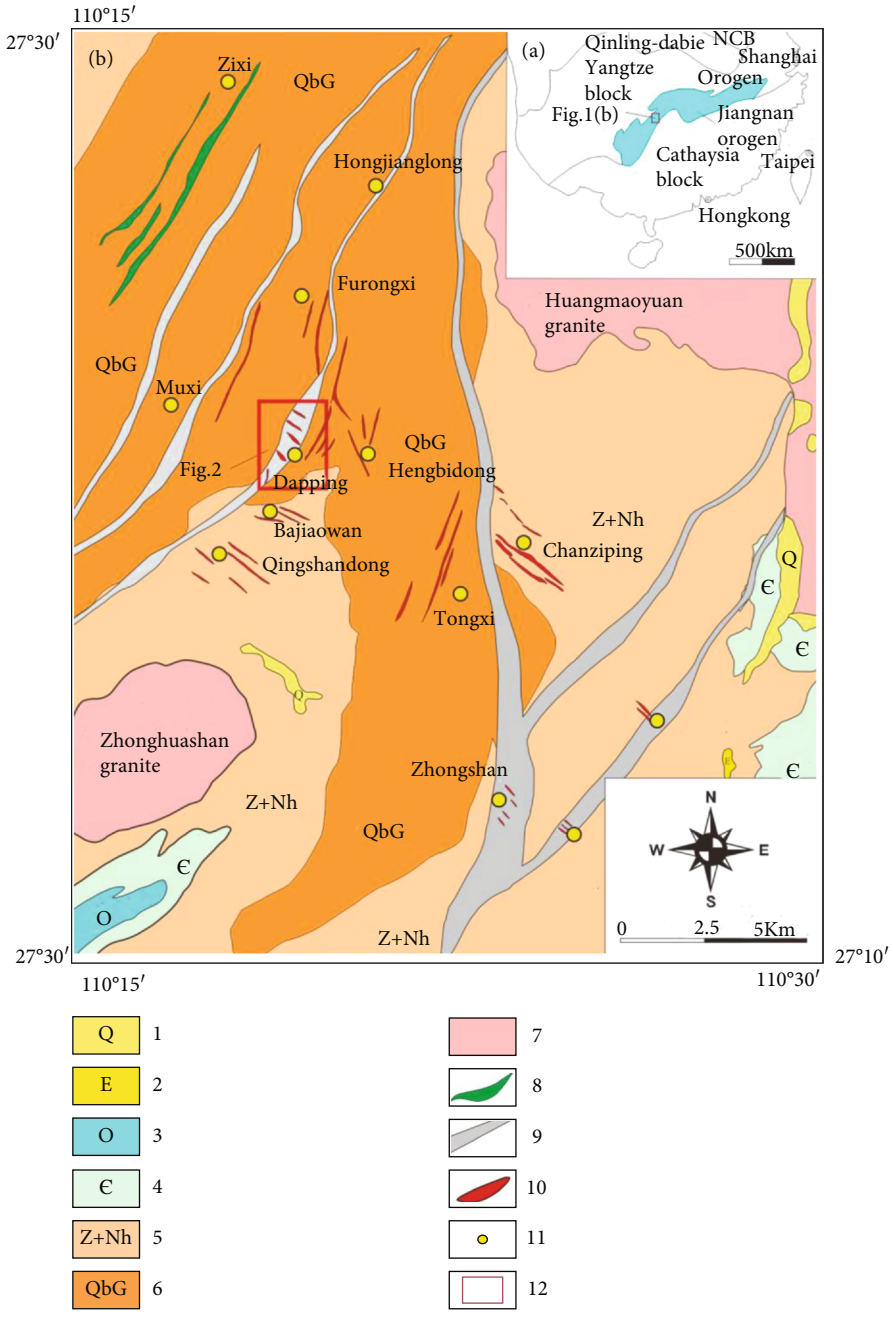

Figure 1: (a) Major tectonic blocks of China. (b) Regional geological sketch map of the middle Xuefeng Mountain (modified after [6–8]): 1: Quaternary (Q); 2: Palaeogene (E); 3: Ordovician (O); 4: Cambrian (Є); 5: Sinian and Nanhuan (Z+Nh); 6: Gaojian Group (QbG); 7: Early Triassic granite rocks; 8: Mafic-ultramafic rocks; 9: shear zone; 10: auriferous vein; 11: gold occurring spot; 12: study area.

them, the Chanziping gold deposit [9–13] and the Daping gold deposit [14] have a scale of large size and medium size, respectively. The exploration of the Daping gold deposit began in 1987 [15] and has proved gold reserves of more than 10 tons. Previous studies on the geological characteristics and metallogenic chronology indicate that the Daping gold deposit belongs to the shear zone type [16, 17] with ore-forming age of 204.8 Ma which belongs to Indosinian [18]. However, the ore-forming fluids, geochemical characteristics of the main and trace elements, rare earth elements, and isotopes of the deposit have not been systematically studied, and its metallogenic mechanism and process are still unknown.

This paper attempts to reveal the source of metallogenic materials, metallogenic mechanism, and deposit type of the Daping gold deposit by petrogeochemistry, H-O-S isotopes, and ore-forming fluids and provide more metallogenic information for further exploration and prediction of the Daping gold deposit and other similar gold deposits with the same metallogenic characteristics.

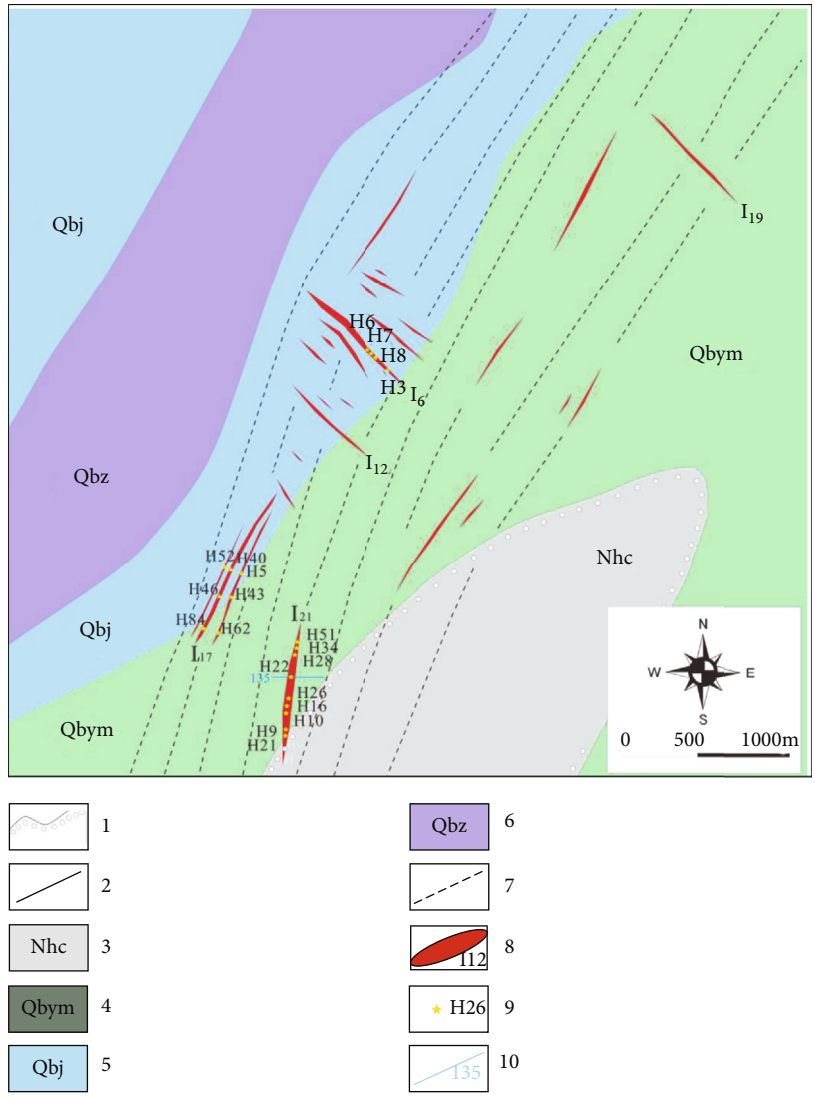

Figure 2: Geological sketch map of the Daping gold deposit (modified after [59]): 1: unconformity boundary; 2: conformity boundary; 3: Changan Formation (Nhc); 4: Yanmenzhai Formation (Qbym); 5: Jiajiantian Formation (Qbj); 6: Zhuanqiangwan Formation (Qbz); 7: ductile-brittle shear zone; 8: auriferous vein; 9: sample location; 10: prospecting line. Due to all the samples coming from diamond drills, only the horizontal positions are shown.

2. Regional Geological Setting

Daping gold deposit which is located in the transitional zone between Yangtze plate and Cathaysia plate belongs to the middle Xuefeng metallogenic belt (Figure 1(a)). The regional strata are composed of Quaternary, Palaeogene, Ordovician, Cambrian, Sinian, Nanhua System, and Gaojian Group of Qingbaikou System (Figure 1(b)). Among these strata, the Gaojian Group of the Qingbaikou System and the Nanhua Systems which belong to low-grade metamorphic greenschist facies clastic rocks with high gold-bearing background values are the main ore-bearing strata in the gold metallogenic belt of the middle Xuefeng Mountain [19]. Frequent acid magmatic activities occurred in this area during the Indosinian period (e.g., Zhonghuashan granite and Huangmaoyuan granite, Figure 1(b)). In addition, six NE-trending or NNE-trending ductile shear zones cross the middle Xuefeng Mountain gold field with length of 10–25 km and width of 0.5–2 km.

3. Geological Characteristics of Daping Gold Deposit

3.1. Deposit Features. The stratum of the Daping gold deposit is composed of the Gaojian Group of the Qingbaikou System and Changan Formation of the Nanhua System, and the gold-bearing faults are NE-trending, NW-trending [20, 21], and NNE-trending. Crossing through the middle part of the study area (Figure 2), the NE-trending ductile-brittle shear cleavage zone may serve as the ore-forming fluid passageways as well as auriferous host structures.

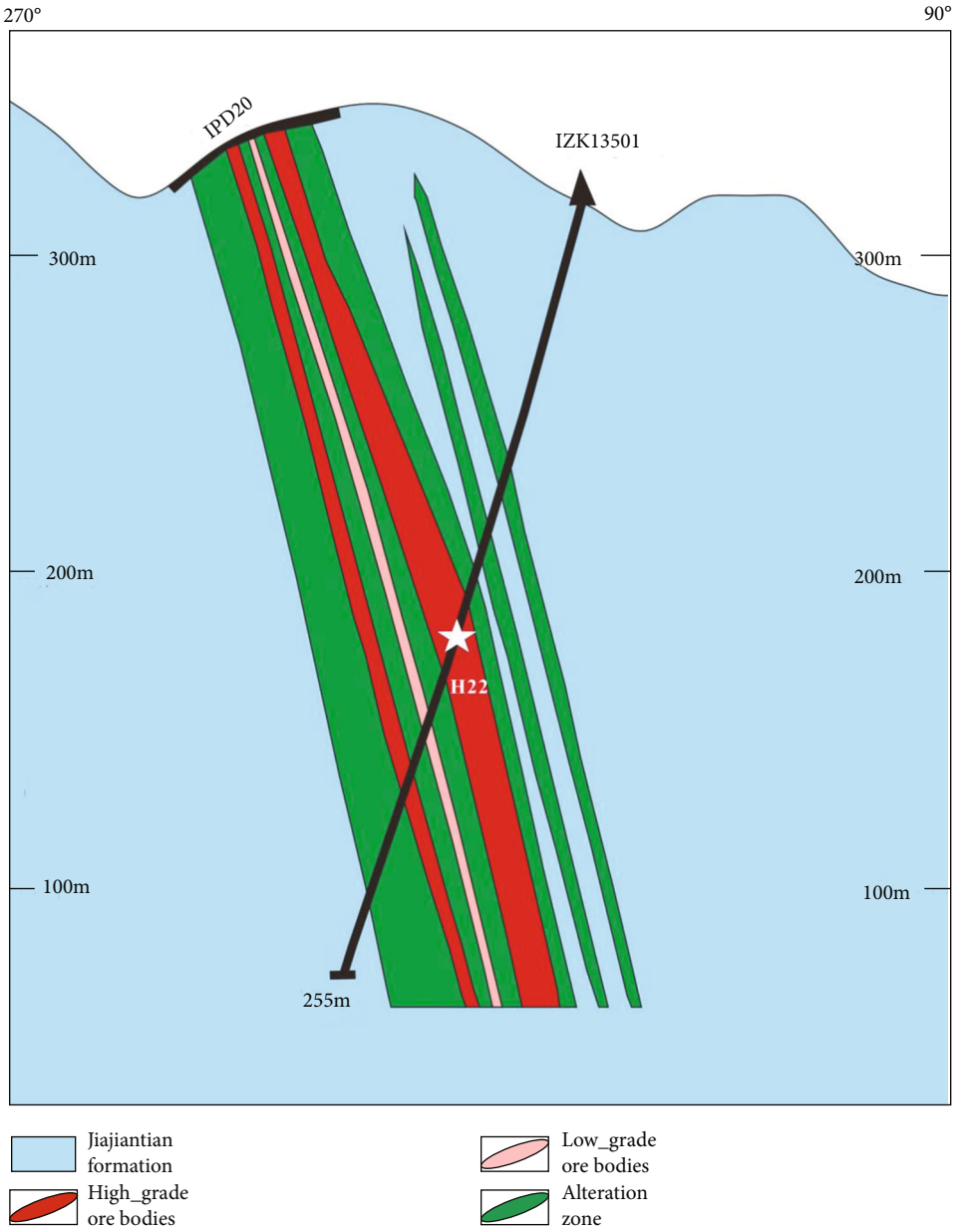

Figure 3: Geologic cross-section (prospecting line 135) of the Daping gold deposit (modified after [59]).

3.2. The Orebody Characteristics. At present, 23 auriferous veins were found out with a length of 120–2100 m and a width of 1.30–70 m. The auriferous veins which occurred in the ductile shear zone or adjacent fault segments are NW-trending of I_6, I_7, I_9, I_{12}, and I_{19} or NE-NNE-trending of I_{17}, I_{20}, I_{21}, and I_{26}. The NW-trending veins intersect the NE-trending vein at a large angle, and both the NE-trending and NW-trending auriferous veins have inclination angles of above 70° (Figure 3). At present, 38 ore bodies have been found out between the elevation of -40 m and 340 m, and among them, 7 main ore bodies have lengths of 170–470 m with an average thickness of 1.36–4.85 m and an average grade of 1.63–25.80 ppm. The alteration types of the Daping gold ores include silicification, sericitization, chloritization, carbonization, and clayization (Figures 4(a), 4(c), and 4(h)). The intensity of silicification, pyritization, and sericitization has positive relations with the intensity of gold mineralization.

3.3. Ore Characteristics. According to the differences of gold-bearing structures, the Daping gold ores can be divided into quartz vein type (gold mineralization mainly occurred in quartz veins and nearby metal sulfides), altered rock type (gold mineralization mainly occurred in alteration rocks), and tectonic breccia type (gold mineralization mainly occurred in tectonic breccia rocks) (Figure 5). The metal minerals of ores are composed of pyrite, arsenopyrite, chalcopyrite, galena, sphalerite, and stibnite, and among them,

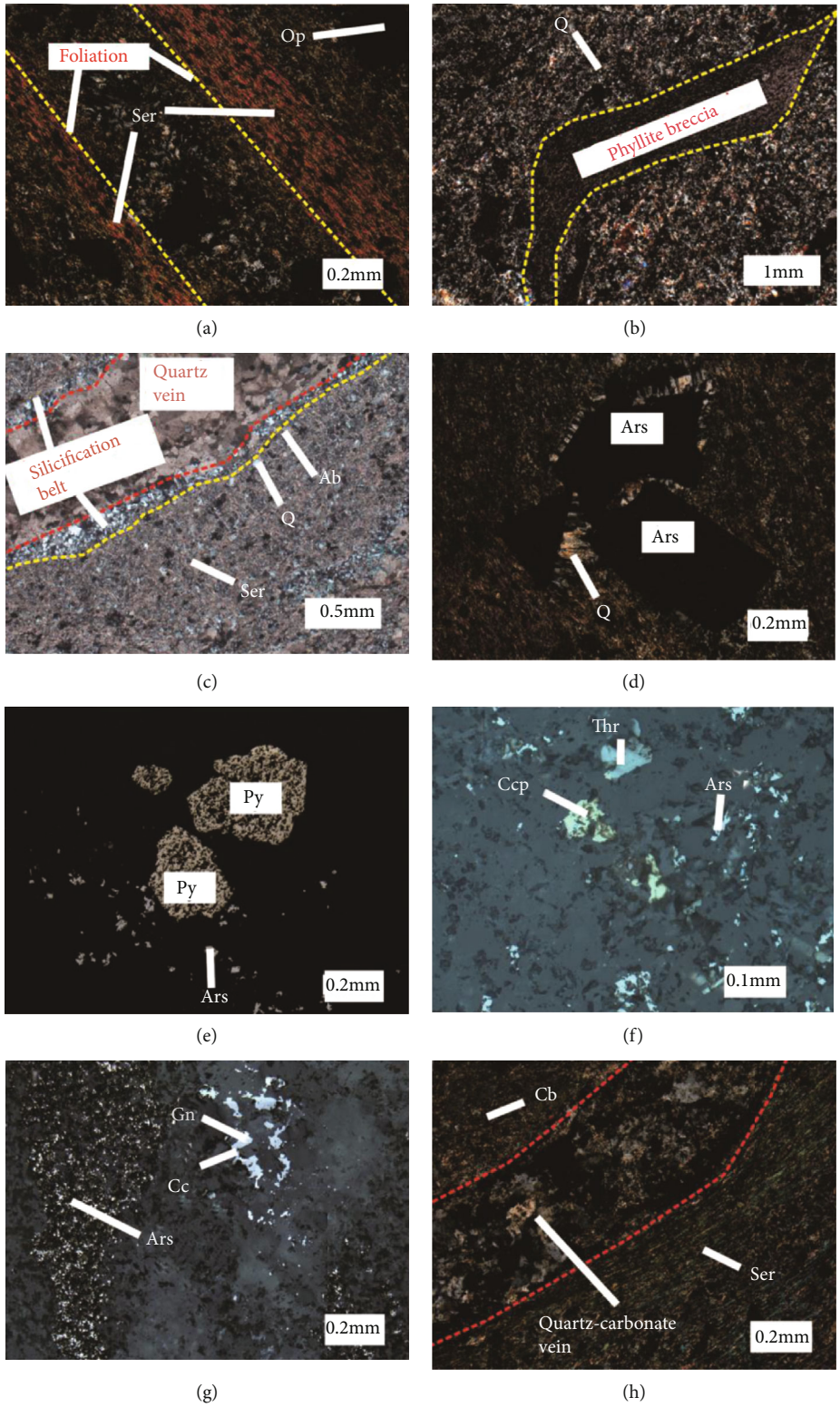

Figure 4: Photomicrographs and microstructures of the Daping gold deposit. (a) The schistose foliation formed by the orientation of sericite (cross-polarized light). (b) Tensile ductile deformation of the phyllite breccia (cross-polarized light). (c) The silicification belt around the quartz vein (plane-polarized light). (d) The pressure shadow (recrystallized quartz) formed by the arsenopyrite (cross-polarized light). (e) The quartz vein containing hypidiomorphic pyrite and xenomorphic arsenopyrite of the first stage of the metallogenic period (reflected light). (f) The quartz vein containing mineral assemblages of xenomorphic arsenopyrite, chalcopyrite, and tetrahedrite of the second stage of the metallogenic period (reflected light). (g) The quartz-carbonate vein of the third stage of the metallogenic period (cross-polarized light). Mineral abbreviation: Py: pyrite; Ars: arsenopyrite; Cc: chalcocite; Gn: galena; Ccp: chalcopyrite; Thr: tetrahedrite; Q: quartz; Ser: sericite; Ab: albite; Cb: carbonate mineral; Op: opaque mineral.

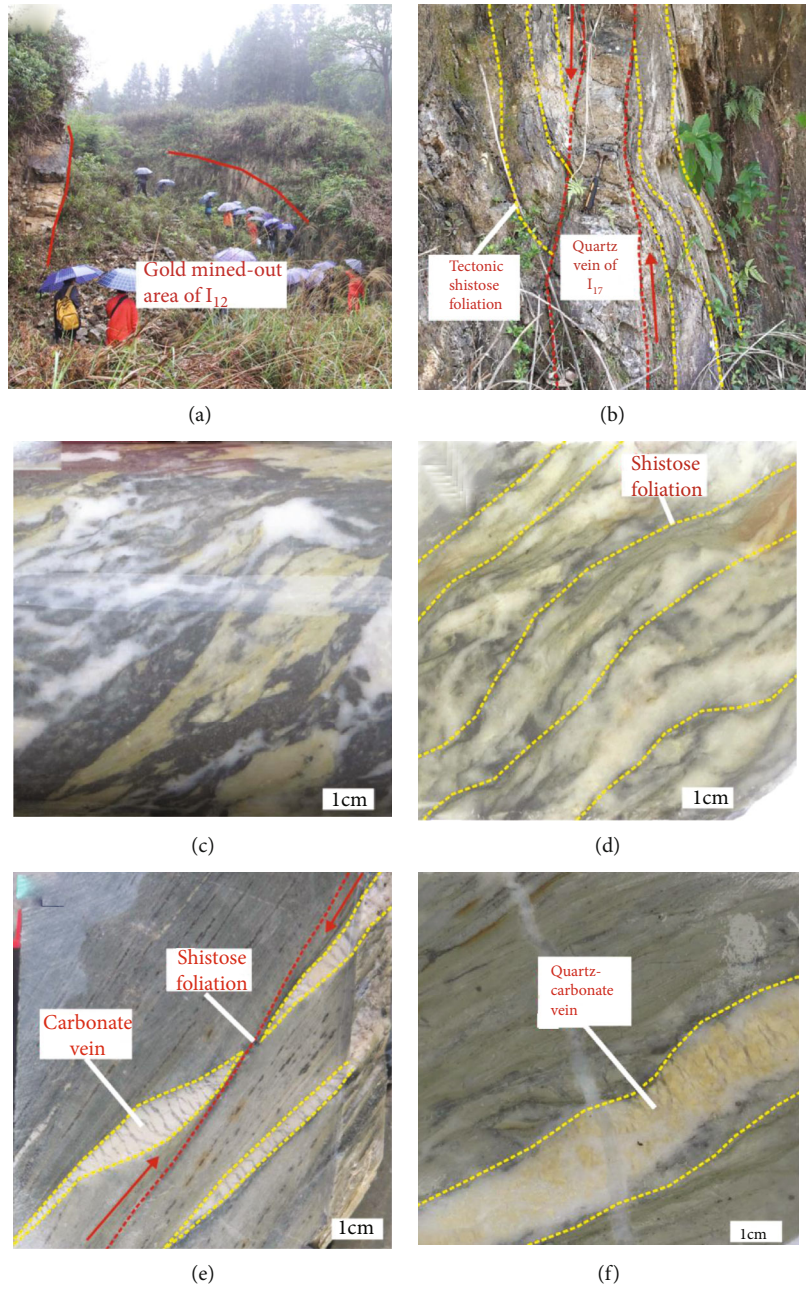

Figure 5: Macroscopic images of auriferous veins and deformation characteristics of the Daping gold deposit. (a) Field image of the NW-trending veins of I_{12}. (b) Macroscopic image of the NE-trending veins of I_{17} shows distinct features of sinistral shear deformation. (c) Irregular quartz breccia and sericite slate breccia of I_{21} vein formed in the tectonic shearing environment. (d) The schistose foliation formed by the orientation of the sericite shows ductile deformation in the I_{21}. (e) The tensile-shearing space was filled by carbonate veins. (f) Quartz-carbonate veins show undulating edge of ductile deformation.

Table 1: Mineral assemblages of ore-forming stages and characteristics of the fluid inclusions.

Period	Stage	Mineral assemblages	Sample No.	Type of the fluid inclusions	Size of the fluid inclusions (μm)	Composition of liquid phase	Composition of gas phase	V/T (%) (20°C)
Metallogenic period	The first stage	Q+Py+Ars±Cb	H28-S1, H43-S1	Two-phase+liquid phase	4.1–12.5	H_2O	H_2O	14–28
	The second stage	Q+polymetallic sulfide minerals (Py, Ars, Cc, Gn, Ccp, Thr)±Chl±Cb	H10-S2, H21-S2, H28-S2, H43-S2	Two-phase+liquid phase+gas phase	2.5–17.8	H_2O	H_2O, CO_2	7–45
	The third stage	Q+Cb	H7-S3, H10-S3	Two-phase+gas phase	2.8–5.1	H_2O	H_2O, CO_2	5–20
Supergene period	Supergene stage	Limonite±patina						

Notes: Py: pyrite; Ars: arsenopyrite; Cc: chalcocite; Gn: galena; Ccp: chalcopyrite; Thr: tetrahedrite; Q: quartz; Chl: chlorite; Cb: carbonate minerals; V/T: vapor/total ratio of two-phase inclusions.

Table 2: Detail location and descriptions of the samples of the Daping gold deposit. The thickness and content of gold of the samples are from [59].

Sample	Auriferous vein	Sampling location	Thickness (m)	Content of gold (ppm)	Rock name
H3	I_6	ZK3201 drilling core 198 m	1.07	1.19	Sericite phyllite
H6	I_6	ZK2802 drilling core 210 m	0.89	0.84	Sericite phyllite
H7	I_6	ZK2802 drilling core 212 m	0.90	1.45	Sericite phyllite
H8	I_6	ZK2802 drilling core 214 m	1.02	0.26	Sericite phyllite
H5	I_{17}	ZK11701 drilling core 86 m	1.07	1.39	Sericite phyllite
H40	I_{17}	ZK11701 drilling core 191 m	0.94	2.94	Sericite phyllite
H52	I_{17}	ZK11701 drilling core 222 m	0.89	1.16	Sericite phyllite
H43	I_{17}	ZK12101 drilling core 211 m	1.16	1.11	Sericite phyllite
H46	I_{17}	ZK12101 drilling core 232 m	1.31	1.21	Sericite phyllite
H62	I_{17}	ZK12501 drilling core 232 m	0.84	1.13	Sericite phyllite
H84	I_{17}	ZK12501 drilling core 414 m	0.99	0.61	Sericite phyllite
H28	I_{21}	ZK13301 drilling core 238 m	1.10	6.78	Sericitolite
H34	I_{21}	ZK13301 drilling core 248 m	0.85	10.77	Sericitolite
H51	I_{21}	ZK13301 drilling core 290 m	1.16	1.86	Sericite phyllite
H22	I_{21}	ZK13501 drilling core 144 m	1.00	3.28	Sericite phyllite
H10	I_{21}	ZK13901 drilling core 138 m	1.35	8.21	Mylonite
H16	I_{21}	ZK13901 drilling core 152 m	1.18	1.47	Sericite phyllite
H26	I_{21}	ZK13902 drilling core 324 m	0.90	5.95	Sericite phyllite
H9	I_{21}	ZK14101 drilling core 211 m	1.08	2.93	Sericite phyllite

Table 3: Average content of the major elements of the Daping gold deposit (wt.%).

Sample	SiO_2	Al_2O_3	TFe_2O_3	CaO	MgO	K_2O	Na_2O	TiO_2	P_2O_5	MnO	SO_3	LOI	Total
H3	75.67	11.65	3.62	1.49	0.97	2.59	1.50	0.36	0.07	0.08	3.17	0.87	102.04
H5	73.11	13.14	2.32	1.22	0.60	1.44	4.78	0.33	0.04	0.05	0.23	2.41	99.67
H6	67.56	12.61	4.83	3.17	1.82	3.93	0.12	0.41	0.14	0.21	3.81	2.58	101.19
H7	67.45	13.31	5.94	2.00	1.37	2.07	3.62	0.40	0.09	0.14	5.92	1.33	103.64
H8	69.58	13.98	3.72	1.06	1.06	3.40	1.80	0.47	0.08	0.10	0.81	3.46	99.52
H26	71.68	10.23	6.30	1.86	1.31	2.61	0.87	0.40	0.03	0.09	3.54	0.96	99.88
H28	76.50	7.86	5.76	1.64	0.91	1.82	0.99	0.29	0.12	0.06	3.90	0.94	100.79
H34	67.98	12.09	7.88	0.88	0.96	2.86	1.50	0.47	0.05	0.06	5.46	0.55	100.74
H40	70.61	12.62	5.24	1.32	0.86	2.93	1.75	0.50	0.09	0.07	4.42	0.53	100.94
H43	65.89	17.06	4.73	1.24	1.14	4.18	2.23	0.65	0.14	0.12	1.17	1.86	100.41
H46	66.49	14.54	4.51	2.90	1.78	3.56	1.32	0.57	0.13	0.12	2.06	2.22	100.2
H51	64.79	15.53	5.86	1.77	1.57	3.68	1.76	0.66	0.08	0.12	1.43	1.81	99.06
H52	65.36	13.17	4.69	3.82	1.90	3.46	1.28	0.41	0.09	0.23	1.80	3.64	99.85
H62	65.75	14.32	4.31	3.41	1.80	3.85	1.22	0.50	0.08	0.19	1.12	3.46	100.01
H84	60.93	18.18	4.77	2.99	1.59	4.66	1.30	0.68	0.08	0.14	2.61	2.81	100.74
Average	68.62	13.35	4.97	2.05	1.31	3.14	1.74	0.47	0.09	0.12	2.76	1.96	

Table 4: Content of trace elements of the Daping gold deposit (ppm).

Sample	H3	H5	H6	H7	H8	H26	H28	H34	H40	H43	H46	H51	H52	H62	H84	Average
Li	20.40	7.20	14.60	9.50	12.40	6.10	6.40	6.00	6.30	9.40	13.40	10.50	6.60	9.40	11.10	9.95
Sc	8.00	9.70	9.40	10.10	11.00	8.60	6.00	9.30	10.70	14.10	11.80	14.60	9.90	10.50	13.50	10.48
V	27.00	17.00	30.00	28.00	56.00	50.00	36.00	57.00	51.00	68.00	59.00	77.00	36.00	50.00	69.00	47.40
Cr	35.00	8.00	21.00	24.00	35.00	31.00	34.00	33.00	25.00	25.00	32.00	40.00	13.00	18.00	26.00	26.67
Co	4.80	3.10	5.40	8.20	10.80	8.30	7.60	7.70	8.50	9.30	9.30	11.20	5.60	7.10	8.80	7.71
Ni	10.60	3.90	11.40	16.70	14.00	12.30	11.70	13.00	10.60	11.40	17.70	17.20	6.00	8.70	10.80	11.73
Cu	7.00	5.30	2.60	7.70	22.40	16.00	9.30	7.10	14.60	25.90	15.20	19.70	8.60	11.70	12.80	12.39
Zn	25.00	57.00	15.00	16.00	22.00	49.00	31.00	24.00	17.00	22.00	20.00	66.00	18.00	17.00	21.00	28.00
Ga	16.90	13.65	17.85	16.10	20.60	14.55	10.20	15.05	16.40	21.20	18.25	20.40	17.55	17.60	23.90	17.35
Rb	88.40	49.40	121.50	69.90	111.50	90.60	60.60	93.70	97.10	128.50	113.50	124.00	111.00	118.00	148.50	101.75
Sr	102.50	165.50	121.00	143.00	97.10	211.00	175.00	142.00	128.00	136.50	194.00	204.00	163.50	200.00	190.50	158.24
Nb	9.60	9.30	11.40	10.70	11.10	6.60	4.60	7.20	8.00	10.70	9.20	10.10	8.50	8.90	11.50	9.16
Cs	15.65	2.85	10.20	4.70	6.10	5.12	3.38	5.16	6.12	7.86	8.89	6.00	6.64	6.90	9.66	7.02
Ta	0.62	0.66	0.63	0.61	0.63	0.41	0.25	0.39	0.56	0.63	0.57	0.63	0.53	0.62	0.77	0.57
Tl	0.41	0.26	0.53	0.32	0.46	0.39	0.26	0.40	0.44	0.57	0.51	0.51	0.48	0.51	0.66	0.45
Bi	0.20	0.16	0.27	0.68	0.92	0.23	0.29	0.18	0.39	0.25	0.35	0.21	0.16	0.20	0.15	0.31
Th	6.52	9.02	8.01	7.99	9.01	5.57	4.34	6.37	6.99	9.77	9.17	8.87	7.47	9.49	11.30	7.99
U	1.40	1.97	1.95	1.77	1.98	0.99	0.79	1.17	1.36	1.84	1.72	1.68	1.58	1.95	2.14	1.62
Zr	194.00	234.00	213.00	191.00	212.00	125.00	96.00	145.00	177.00	242.00	218.00	195.00	209.00	205.00	262.00	194.53
Hf	5.80	7.20	6.30	5.80	6.50	3.70	2.90	4.40	5.20	7.20	6.40	5.80	6.10	6.00	7.90	5.81
$w(U)/w(Th)$	0.21	0.22	0.24	0.22	0.22	0.18	0.18	0.18	0.19	0.18	0.19	0.19	0.21	0.21	0.19	0.20
$w(Rb)/w(Sr)$	0.86	0.30	1.00	0.49	1.15	0.43	0.35	0.66	0.76	0.94	0.59	0.61	0.68	0.59	0.78	0.68
$w(Co)/w(Ni)$	0.45	0.79	0.47	0.49	0.77	0.67	0.65	0.59	0.80	0.82	0.53	0.65	0.93	0.82	0.81	0.68
$w(Zr)/w(Hf)$	33.45	32.50	33.81	32.93	32.62	33.78	33.10	32.95	34.04	33.61	34.06	33.62	34.26	34.17	33.16	33.47

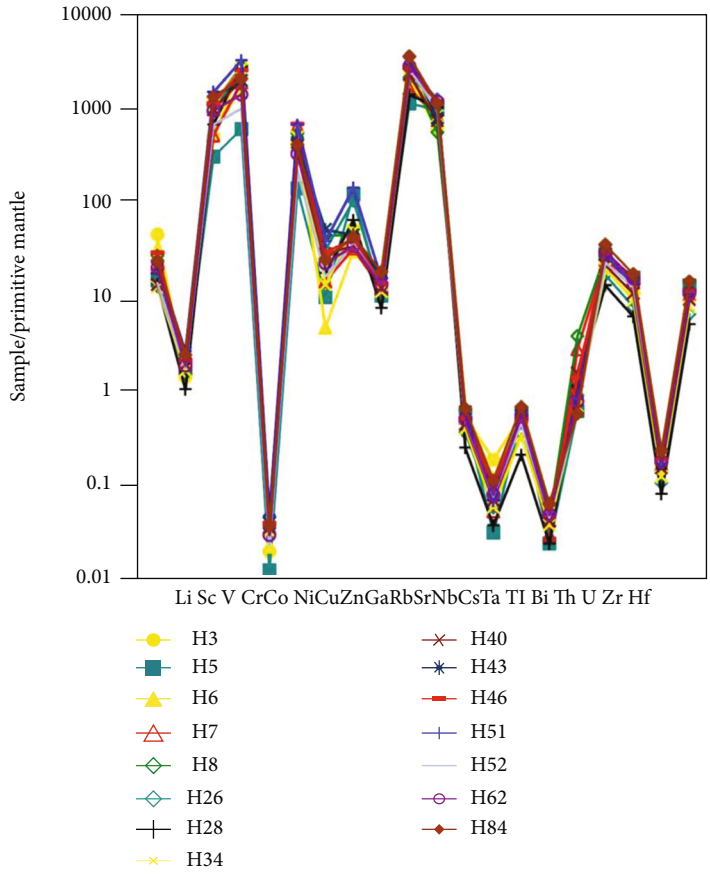

Figure 6: Primitive standard spider graph of trace elements of Daping gold deposit. The values for primitive mantle are from [62].

pyrite and arsenopyrite are the main gold-bearing minerals. The gangue minerals are mainly including quartz, carbonate minerals, albite, sericite, and muscovite.

According to the mineral assemblages, the metallogenic process of the Daping gold deposit can be divided into two periods (metallogenic period and supergene period) and four stages (Table 1, Figure 4). The first stage has mineral assemblages of quartz+pyrite+arsenopyrite±carbonate minerals and the second stage has mineral assemblages of quartz+polymetallic sulfide minerals (pyrite, arsenopyrite, chalcocite, galena, chalcopyrite, tetrahedrite)±chlorite±carbonate minerals which are the main gold mineralization stages. The third stage has mineral assemblages of quartz and carbonate minerals. The supergene stage is characterized by the mineral of limonite±patina which is formed by the oxidation of metal sulfides.

4. Sampling and Analytical Methods

4.1. Samples. The nineteen samples which were collected from drill holes are used for the geochemical and metallogenic study of the Daping gold deposit. Samples H3, H6, H7, and H8 from auriferous vein I_6 are sericite phyllite with gold content of 0.26–1.19 ppm. Samples H5, H40, H52, H43, H46, H62, and H84 from auriferous vein I_{17} are sericite phyllite with gold content of 0.61–2.94 ppm. Samples H28, H34, H51, H22, H10, H16, H26, and H9 from auriferous vein I_{21} are sericite phyllite, sericitolite, and mylonite with gold content of 1.47–10.77 ppm. For detailed sample information, see Table 2 and Figure 2.

4.2. Analytical Methods. The major elements and trace element of whole rock were tested in samples H3, H5, H6, H7, H8, H26, H28, H34, H40, H43, H46, H51, H52, H62, and H84. Hydrogen and oxygen isotopes of mineral quartz were tested in samples H28, H34, H22, H10, H16, H26, H9, and H46. Sulfur isotope of arsenopyrite and pyrite was tested in samples H34, H22, H16, H26, H7, and H46. The homogenization temperature, freezing temperature, and laser Raman spectra of the ore-forming fluid inclusions were tested in samples H7, H10, H21, H28, and H43.

The major elements, trace element, and isotopes of sulfur, hydrogen, and oxygen of the Daping gold ore samples were measured in the Australian Real Analysis Test (Guangzhou) Co., Ltd. The major elements were tested by the X-ray fluorescence instrument of ME-XRF26d with precision and accuracy better than ±5%. The trace elements and the rare earth elements are measured by instruments of M61-MS81, and the relative error is less than 10%. Sulfur isotope was measured by an instrument of S-ISTP01L with accuracy of better than 0.02%. Hydrogen isotope was tested by the instrument of H-ISTP01 with accuracy of better than 0.3%. The oxygen isotope was measured by the instrument of O-ISTP01 with accuracy of better than 0.03%. $\delta^{18}O_{H_2O}$ were

Table 5: Content of rare earth elements of the Daping gold deposit (ppm).

Sample	H3	H5	H6	H7	H8	H26	H28	H34	H40	H43	H46	H51	H52	H62	H84	Average
La	31.00	35.50	45.00	39.90	36.10	20.50	20.90	26.00	29.00	38.40	33.40	33.70	31.80	33.60	39.20	32.93
Ce	64.40	74.20	90.40	81.60	75.60	43.10	42.40	53.40	61.00	80.10	69.50	70.20	67.10	67.60	82.30	68.19
Pr	7.09	8.06	9.89	8.55	8.05	4.61	4.56	5.83	6.55	8.64	7.57	7.60	7.28	7.15	8.92	7.36
Nd	26.40	29.20	37.30	31.10	29.10	17.00	16.40	21.80	23.90	31.90	27.60	28.30	27.20	25.80	32.30	27.02
Sm	5.83	5.94	7.85	6.33	6.34	3.50	3.43	4.54	4.99	6.75	5.96	5.93	5.87	5.33	6.77	5.69
Eu	1.16	0.96	1.92	1.24	1.30	0.74	0.69	0.96	1.01	1.45	1.29	1.27	1.17	1.15	1.47	1.19
Gd	5.12	5.06	7.70	5.12	5.85	3.22	2.89	4.00	4.18	5.64	4.91	5.16	5.41	4.87	5.69	4.99
Tb	0.88	0.78	1.19	0.80	0.92	0.48	0.45	0.63	0.68	0.90	0.77	0.84	0.85	0.78	0.87	0.79
Dy	5.09	4.87	6.64	4.67	5.60	2.92	2.55	3.64	4.12	5.43	4.82	5.05	5.21	4.58	5.51	4.71
Ho	1.07	1.06	1.39	0.97	1.15	0.63	0.53	0.75	0.84	1.12	0.99	1.01	1.10	0.96	1.15	0.98
Er	3.27	3.14	4.06	3.01	3.40	1.83	1.48	2.16	2.38	3.25	2.89	2.98	3.14	2.82	3.31	2.87
Tm	0.49	0.49	0.63	0.48	0.53	0.27	0.23	0.33	0.38	0.50	0.45	0.45	0.47	0.42	0.52	0.44
Yb	3.28	3.23	4.14	3.22	3.77	1.92	1.47	2.18	2.53	3.40	2.88	3.11	3.21	2.86	3.37	2.97
Lu	0.47	0.49	0.65	0.52	0.57	0.29	0.22	0.33	0.38	0.50	0.45	0.48	0.48	0.43	0.53	0.45
Y	33.20	29.60	42.60	29.40	33.50	18.30	15.60	21.60	24.60	31.70	29.40	30.20	31.40	28.30	33.30	28.85
ΣREE	155.55	172.98	218.76	187.51	178.28	101.01	98.20	126.55	141.94	187.98	163.48	166.08	160.29	158.35	191.91	160.58
LREE	135.88	153.86	192.36	168.72	156.49	89.45	88.38	112.53	126.45	167.24	145.32	147.00	140.42	140.63	170.96	142.38
HREE	19.67	19.12	26.40	18.79	21.79	11.56	9.82	14.02	15.49	20.74	18.16	19.08	19.87	17.72	20.95	18.20
w(LREE)/w(HREE)	6.91	8.05	7.29	8.98	7.18	7.74	9.00	8.03	8.16	8.06	8.00	7.70	7.07	7.94	8.16	7.82
w(La) N/w(Yb) N	6.78	7.88	7.80	8.89	6.87	7.66	10.20	8.55	8.22	8.10	8.32	7.77	7.11	8.43	8.34	7.95
δEu	0.65	0.54	0.75	0.67	0.65	0.67	0.67	0.69	0.68	0.72	0.73	0.70	0.63	0.69	0.72	0.68
δCe	1.07	1.08	1.05	1.08	1.09	1.09	1.06	1.06	1.09	1.08	1.07	1.08	1.08	1.07	1.08	1.07

Table 6: Isotopic values of D and O of the Daping gold deposit. The values of the δO_{H_2O} are yielded by the equation: $\delta^{18}O_Q - \delta^{18}O_{H_2O} \approx 3.38 \times 10^6/T^2 - 3.40$ [22].

Sample	Mineral	δD (‰)	$\delta O_{V\text{-}SMOW}$ (‰)	δO_{H_2O} (‰)	T (°C)
H28-OH1	Quartz	-62	11.4	2.72	255.8
H34-OH1	Quartz	-59	14.1	5.42	255.8
H22-OH1	Quartz	-61	10.1	1.42	255.8
H10-OH1	Quartz	-60	11.3	-1.44	184.5
H16-OH1	Quartz	-53	12.9	0.16	184.5
H26-OH1	Quartz	-62	16	3.26	184.5
H9-OH1	Quartz	-61	13.6	0.86	184.5
H46-OH1	Quartz	-51	15.7	2.96	184.5

calculated according to the equation suggested by Clayton et al. [22]: $\delta^{18}O_Q - \delta^{18}O_{H_2O} \approx 3.38 \times 10^6/T^2 - 3.40$.

The homogenization temperature and freezing temperature testing of the ore-forming fluids were conducted by the instrument of LINKAMTHMSG600 in the Fluid Inclusion Laboratory of Chengdu University of Technology with temperature accuracy of ±0.1°C. The salinities of the metallogenic fluid inclusions were calculated by using the equation of [23]: $W = 0.00 + 1.78T_m - 0.042\,T_m{}^2 + 0.000557\,T_m{}^3$, where W is the weight percentage of NaCl (0–23.3% NaCl) and T_m is the freezing point depression (°C). The laser Raman spectra of single fluid inclusion were measured by the instrument of HORIBA LabRAM HR Evolution in the Raman Lab of Chengdu University of Technology with spatial resolution of 1 μm.

5. Analytical Results

5.1. Major Elements. The test results of the major elements illustrate that the Daping gold ores have a high content of SiO_2 and S and low content of Al_2O_3, TiO_2, CaO, Na_2O, MnO, and K_2O (Table 3). With the increasing of gold mineralization, the intensity of silicification alteration and sulfide mineralization increased significantly.

5.2. Trace Element. The trace element analysis results (Table 4) show that the samples have $w(U)/w(Th)$ ratios of 0.18–0.24 (0.20 in average), $w(Rb)/w(Sr)$ ratios of 0.35–1.15 (0.68 in average), $w(Co)/w(Ni)$ ratios of 0.45–0.93 (0.68 in average), and $w(Zr)/w(Hf)$ ratios of 32.50–34.26 (33.47 in average). The content values of U, Rb, and Co in the ores of Daping gold deposit are smaller than Th, Sr, and Ni. The content value of Zr is greater than Hf. The original mantle-standardized spider map shows that the elements of Li, Cr, Ni, Zn, Rb, Th, and Sr enriched obviously, and on the contrary, the elements of Sc, Co, Cu, Ga, Cs, Tl, and Zr were depleted (Figure 6).

5.3. Rare Earth Element. Rare earth elements are important indications for the analysis of the ore-forming material sources due to their stable chemical properties and the specificity of distribution [24]. REE testing results (Table 5) show that the total amount of rare earth element (ΣREE) of the Daping gold ores is 98.20–218.76 ppm (160.58 ppm in average), the total amount of LREE is 88.38–192.36 ppm (142.38 ppm in average), the total amount of HREE is 9.82–26.40 ppm (18.20 ppm in average), the ratio of $w(\text{LREE})/w(\text{HREE})$ is 6.91–9.00 (7.82 in average), and the ratio of $w(La)_N/w(Yb)_N$ is 6.78–10.20 (7.95 in average). The δEu values ranging from 0.54 to 0.75 and the δCe values ranging from 1.05 to 1.09 show positive Ce anomaly and negative Eu anomaly. All of the samples have a similar REE pattern of right-dip type indicating that they may have homologous origins (Figure 6) [25].

Table 7: Isotope values of $\delta^{34}S$ in the arsenopyrite or pyrite of the Daping gold deposit.

Sample	Mineral	$\delta^{34}S$ (‰)
H34-S1	Arsenopyrite	-0.94
H22-S1	Arsenopyrite	-1
H16-S1	Arsenopyrite	-0.76
H26-S1	Arsenopyrite	-0.67
H7-S1	Pyrite	1.98
H46-S1	Pyrite	0.23

5.4. Hydrogen and Oxygen Isotope. The hydrogen and oxygen isotope testing results (Table 6) of quartz mineral samples show that the value of δD_{H_2O} is from -51‰ to 62‰ (-58.6‰ in average), and the value of $\delta^{18}O_{H_2O}$ is from -1.44‰ to 5.42‰ (1.92‰ in average).

5.5. Sulfur Isotope. The sulfur isotope is important for studying the source of ore-forming materials [26, 27]. Six sulfur isotope samples of metal sulfides (pyrite or arsenopyrite) were tested, and the testing results (Table 7) show that the value of $\delta^{34}S$ is from -1.00‰ to 1.98‰ (-0.13‰ in average), which are close to the average S isotope of the magmatic hydrothermal deposit of 1.68‰ [28, 29].

5.6. Ore-Forming Fluid Inclusion Testing. According to the microscope observation, the ore-forming fluid inclusions are in the shape of circle, ellipse, or irregular. The metallogenic period of the Daping gold deposit can be divided into three stages. The inclusions of stage one are two-phase inclusions and liquid phase inclusions. The inclusions of stage

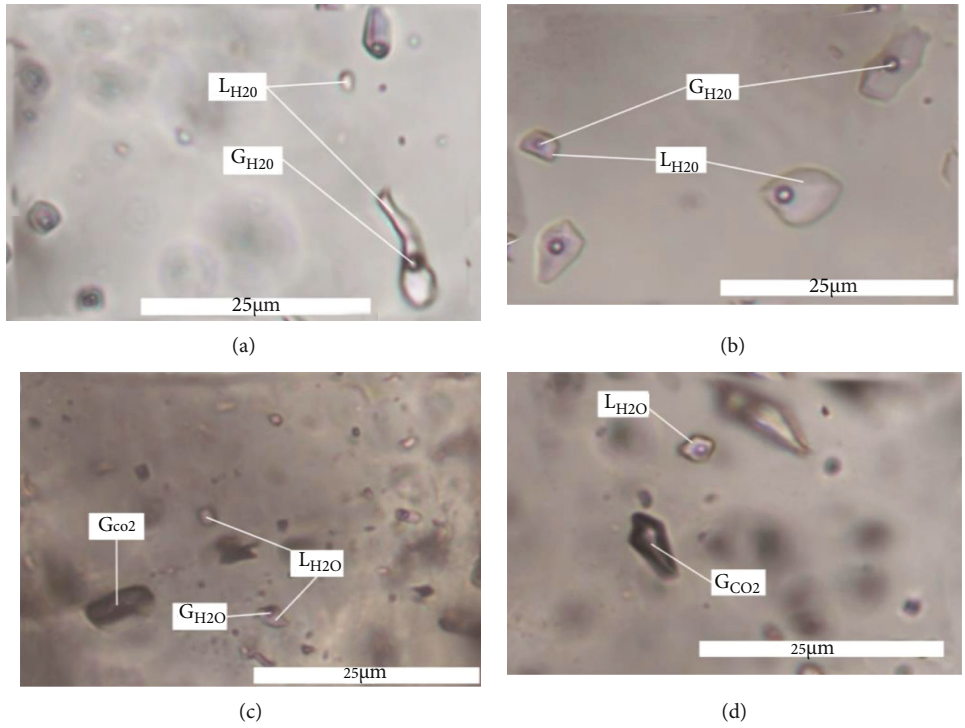

Figure 7: Photomicrographs of the typical fluid inclusions of the Daping gold deposit. (a) Two-phase and liquid phase of the first ore-forming stage. (b) Two-phase inclusions of the first ore-forming stage. (c) Two-phase, liquid phase, and gas phase inclusions of the second ore-forming stage. (d) Two-phase and gas phase inclusions of the third ore-forming stage. Abbreviation: L_{H_2O}: liquid H_2O; G_{H_2O}: vapor H_2O; G_{CO_2}: vapor CO_2.

two are two-phase inclusions, liquid phase inclusions, and gas inclusions. The inclusions of stage three are two-phase inclusions and gas phase inclusions. Based on the laser Raman spectra testing, the composition of the liquid phase inclusions is H_2O, and the composition of the gas phase inclusions is H_2O and CO_2. For detailed characteristics of the fluid inclusions, see Table 1 and Figures 7 and 8.

The first stage of the ore-forming fluid yielded homogenization temperature of 218.0–293.1°C (255.8°C in average) and salinity of 4.98–17.94 wt.% NaCl eqv. (11.35 wt.% NaCl eqv. in average). The second stage of the ore-forming fluid yielded homogenization temperature of 159.3–240.6°C (184.5°C in average) and salinity of 5.28–10.59 wt.% NaCl eqv. (7.64 wt.% NaCl eqv. in average). The third stage of the ore-forming fluid yielded homogenization temperature of 138.5–177.1°C (157.3°C in average) and salinity of 0.71–7.78 wt.% NaCl eqv. (4.82 wt.% NaCl eqv. in average). For details of the fluid inclusion testing, see Table 8 and Figure 9.

6. Discussion

6.1. Source of Ore-Forming Materials and Fluids. The Pre-Cambrian basement of the middle Xuefeng Mountain area is composed of Lengjiaxi Group, Gaojian Group, and Nanhua System which have average gold content of 19.46 ppb, 41.86 ppb, and 20.51 ppb, respectively [30–32]. The gold content of the base rocks is 6.5–14 times than the average bulk continental crust of 3.0 ppb [33] and thus can provide an abundant initial gold source for the formation of the gold deposits in the middle Xuefeng Mountain area.

Trace element studies show that the Daping gold ores enrich in Li, Cr, Ni, Zn, large ion lithophile elements of Rb and Sr, and high field strength element of Th and deplete in elements of Sc, Co, Cu, Ga, Cs, Tl, and Zr (Figure 6). The chondrite standard distributions of REE curves of gold ores have similar patterns of right-dip indicating that they probably have the same material sources and origins [25]. The rare earth elements of the gold ores are characterized by the strong enrichment of LREE (Figure 10). The δEu values range from 0.54 to 0.75 which show negative Eu anomaly, indicating that Daping gold deposit may form in the reducing environment [24, 34].

On the diagram of $\delta^{18}O_{H_2O}$ vs. δD_{H_2O} (Figure 11), auriferous quartz of the Daping gold ores is mainly located between the magmatic water and meteoric water and partly located at magmatic water, which indicates that the metallogenic fluids may be the mixing fluids of magmatic waters and meteoric water. Considering that the Zhonghuashan granite and Huangmaoyuan granite (belonging to Baimashan complex granites) (Figure 1) are only a few kilometers away from Daping gold deposit and have $\delta^{18}O$ value of 9.74–11.2‰ [35] which overlap partially with $\delta^{18}O$ value of 10.1–15.7‰ of the Daping gold-bearing quart, this indicates that the metallogenic fluids may partly come from the deep concealed granite with mixing of the meteoric water, which is similar to the Chanziping deposit (Figure 12). The $\delta^{34}S$‰ values of sulfide isotope from metal

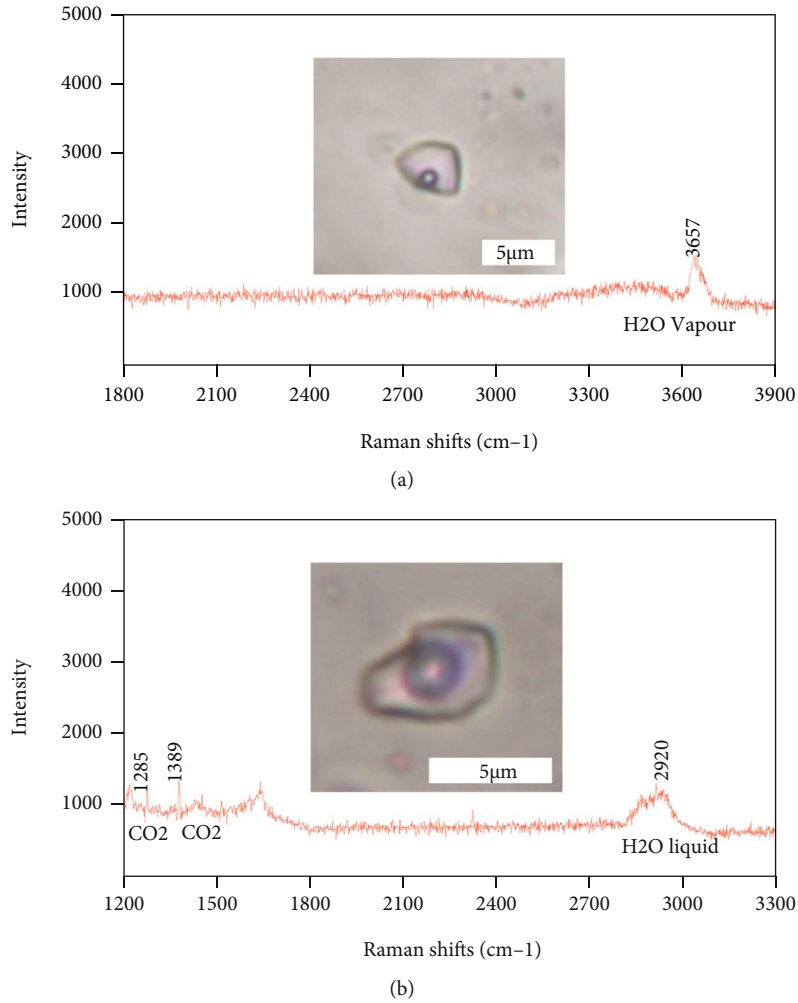

Figure 8: Microstructures and laser Raman spectra for fluid inclusions in Daping gold deposit.

Table 8: Microthermometric data of fluid inclusions of the metallogenic period in the Daping gold deposit.

Stage	Host mineral	Counts	T_h (°C)	Average T_h (°C)	T_m (ice) (°C)	Average T_m (ice) (°C)	Salinity (wt.% NaCl eqv.)	Average salinity (wt.% NaCl eqv.)
The first stage	Quartz	9	218.0–293.1	255.8	From -13.7 to -3.0	-7.6	4.98–17.94	11.35
The second stage	Quartz	39	159.3–240.6	184.5	From -7.0 to -3.2	-4.8	5.28–10.59	7.64
The third stage	Quartz	8	138.5–177.1	157.3	From -4.9 to -0.4	-2.9	0.71–7.78	4.82

T_h: homogenization temperature; T_m (ice): melting temperature of ice. The salinity and density of the fluid inclusions are calculated by the equation of [23].

sulfides of the Daping gold deposit range from -1 to 1.98, which are consistent with the granite; Gaojian Group (Figure 12) implied that both the granite and Gaojian Group may contribute to the sulfur sources.

Most granites in middle Xuefeng Mountain and adjacent regions belong to S-type granites [35–37] and have low gold contents (e.g., the Baimashan complex granites have average gold content of 1.25 ppb [38]). Considering that the magma source of the granites have gold contents of 19.46–41.86 ppb which are much higher than the 1.25 ppb of granites, thus, the gold element may aggregate in the magmatic hydrothermal fluids and may partly contribute to the formation of Mesozoic regional gold deposits.

6.2. Metallogenic Mechanism. Based on Rb-Sr dating of quartz, the Daping gold deposit and Chanziping gold deposit occurred in 204.8 Ma and 205.6 Ma, respectively [18]. Large-scale regional thrusting nappe structures and associated acid magma intrusion activities occurred at 225–201 Ma of the Indosinian period [18, 36, 37]. Thus, the

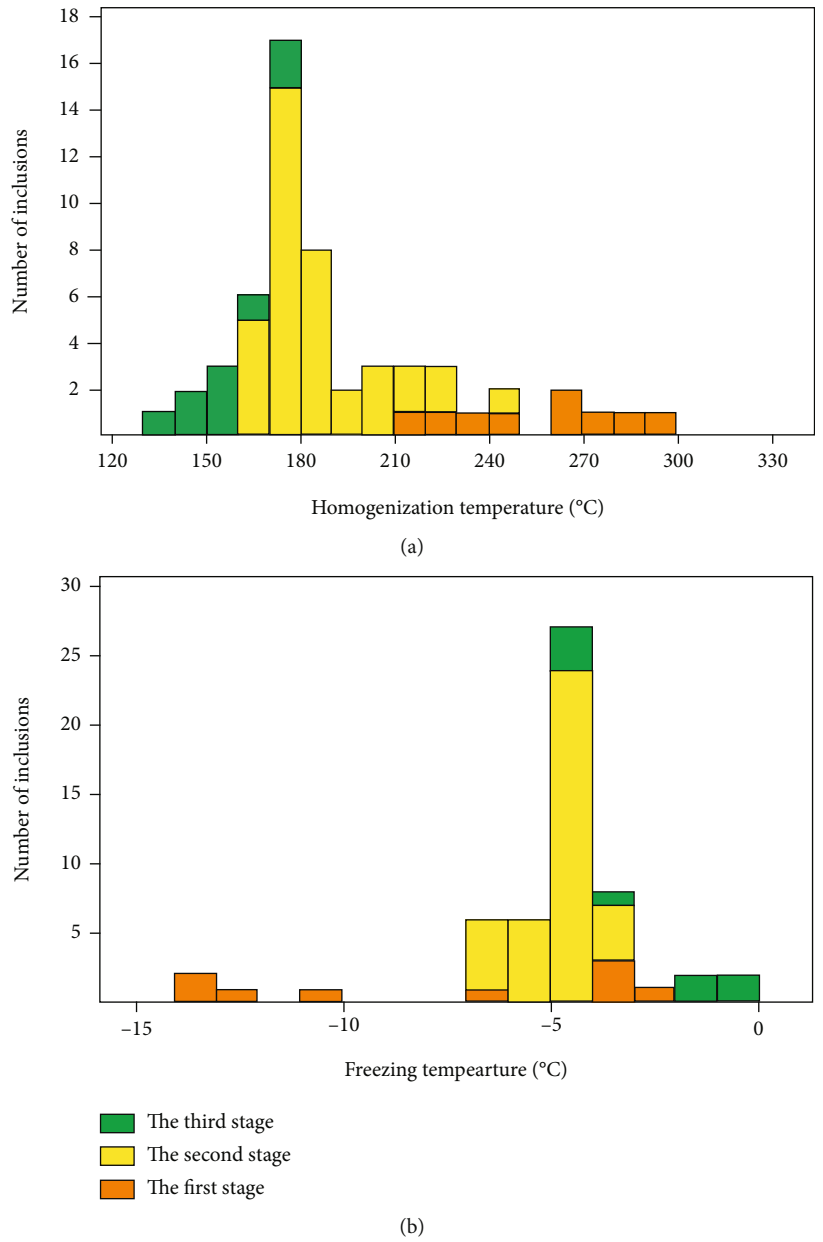

Figure 9: (a) Frequency histogram of the homogenization temperature of the Daping metallogenic fluids. (b) Frequency histogram of the freezing temperature of metallogenic fluids. The homogenization temperature data and freezing temperature data are from microthermometric analysis of the fluid inclusions (this study).

metallogenic epoch of regional gold mineralization is a little younger than the intrusion time of granites.

The tectonic schistose foliation developed in auriferous veins (for example, I_{17} and I_{21}) and ductile deformation of auriferous quartz veins (Figures 5(b), 5(d), and 5(e)) provides important evidence for the existence of brittle and ductile shear zones. The development of tectonic schistose foliation structure provides a migration channel for ore-forming fluids and serves as the main place for the precipitation and enrichment of ore-forming materials [39]. Driven by the thermal gradient of concealed granite, the gold metallogenic fluids migrate along the brittle and ductile shear zones, and in this process, the gold element of the adjacent stratum also adds to the fluids. When the ore-forming fluids reach the shallow stratum, and under the environment of depressurizing and fluid immiscibility, the thermodynamic equilibrium of CO_2 and oxygen fugacity were destroyed, and thus, the gold element precipitated in the quartz and metal sulfides to form the gold ores [16].

6.3. Ore Genetic Type. As an important type of gold deposits in the world, the orogenic gold deposits provide at least 30% of global gold reserves [40], and 17 giant gold deposits (>500 t Au) around the world belong to the orogenic gold type. Since the evolutionary history of the orogenic belt can be recorded in the formation of the orogenic gold

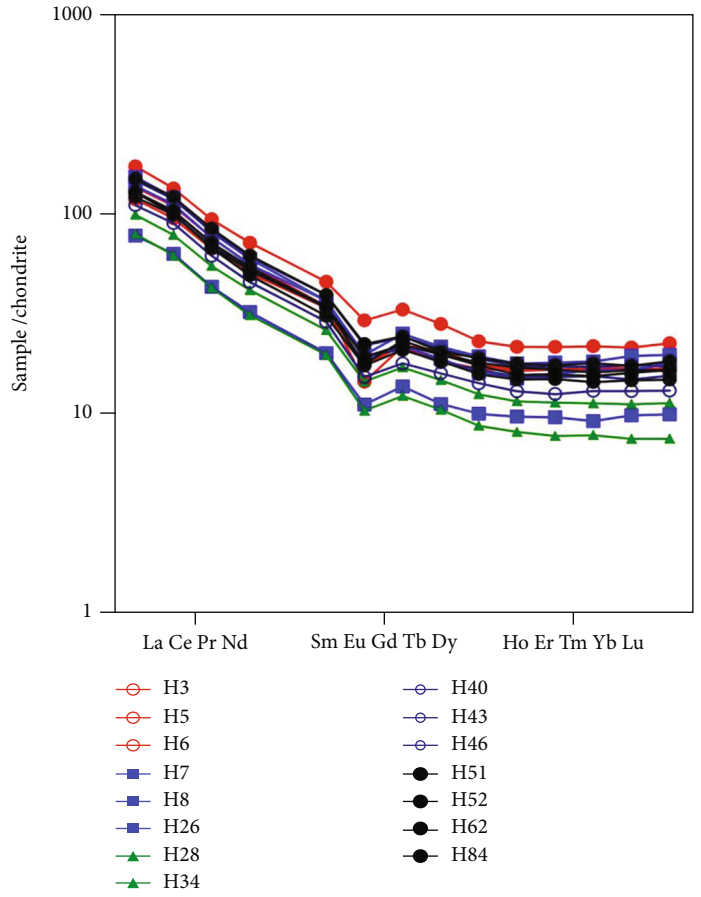

Figure 10: Chondrite meteorite standard distribution pattern of Daping gold deposit. The values for chondrite are from [63].

deposits [41], the study of the ore-forming process and genesis of the orogenic gold deposits can provide valuable information of metamorphism and uplift-erosion process of the orogenic belt and thus attracted more and more geologists to conduct research on such type of gold deposits. Before the jargon of orogenic gold deposits was proposed, the classification of the gold deposits which occurred in the orogenic belts or greenstone belts was in chaos. For instance, based on the differences of the surrounding rocks, the gold deposits were classified into green belt type, turbidite type, and BIF (banded iron formation) type [42]; based on the differences of mineralization characteristics, the gold deposits were classified into quartz vein type, altered rock type, and breccia type [43]; based on the differences of ore-controlling factors, the gold deposits were classified as shear zone type [44]. Groves et al. [45] proposed that the gold deposit formed in the tectonic environment of the squeezing or compression in the convergence region of the plates and has close genetic relationship with the orogenic process which can be classified as orogenic gold deposit, and thus, the gold types mentioned above should be classified as one type of orogenic gold deposit.

The middle Xuefeng Mountain area is located in the transition zone between Cathaysian plate and Yangtze plate and had undergone many periods of crustal tectonic movement and forms a large number of faults and folds as well as a series of ductile-brittle shear zone structures and multiple metallogenic episodes including Paleozoic (e.g., Zixi gold deposit of 425 Ma [46]) and Late Triassic (e.g., Chanziping and Daping gold deposit). In the Indosinian period, due to the strong NW-SE compression tectonic activities and the intrusion activities of regional acidic magmas, the magmatic hydrothermal fluids upwelled along the shear zone, and the gold elements in the stratum were activated, migrated, and gradually precipitated and enriched in the proper weak tectonic structures (for instance, ductile-brittle shear structures).

Similar Mesozoic gold deposits were also reported in the Jiangnan Orogen, e.g., Yanlinsi, Hengjiangchong, Wangu, Huangjindong, Jinjing, Mali, Fenshuiao, and Dayan [1, 4, 47–52]. And generally speaking, its gold mineralization has close spatial relations with regional granitic intrusions [1]. H–O–C–S–Pb isotopic data of ore-forming fluids indicate that its ore-forming materials mainly source from granitic magma and minor from basement metamorphic stratum ([1] and references therein). The ore-controlling structure of the shear zone of Daping gold deposit is similar to many world typical orogenic gold deposits [53–58]. In addition, the Daping gold deposit has many similar characteristics to the typical orogenic gold deposits (Table 9), for instance, the tectonic background of orogen, the ore-bearing rocks of semideep sea or deep sea sediments, the ore-type of quartz

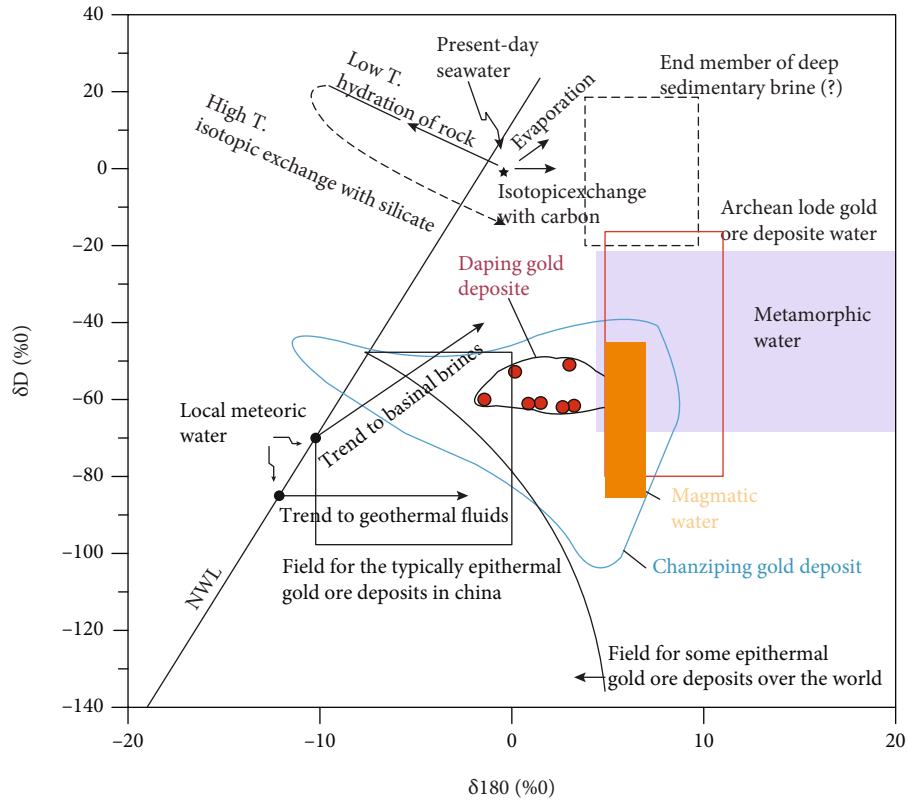

FIGURE 11: Plot of δD_{H_2O} versus $\delta^{18}O_{H_2O}$ of the metallogenic fluids in Daping gold deposit (modified after [1]). Primary magmatic and metamorphic water boxes and meteoric water line are from [64].

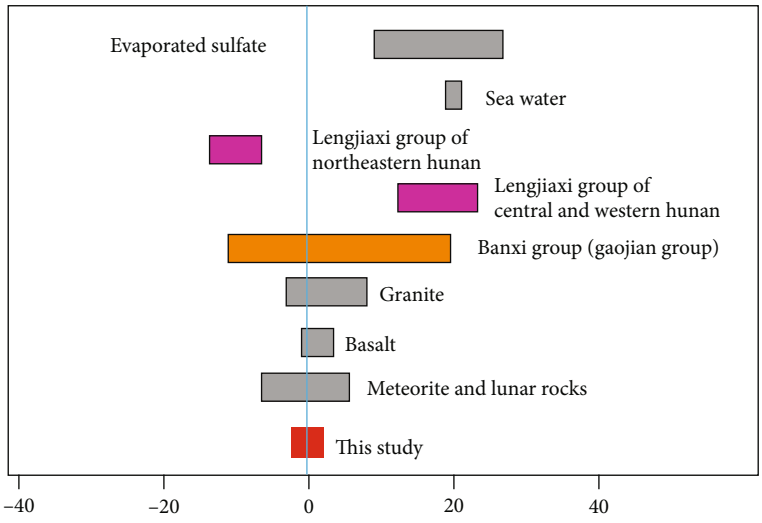

FIGURE 12: Sulfur isotope composition of ores in Daping gold deposit (modified after [46, 65–67]). Data of the Lengjiaxi Group and Banxi Group (Gaojian Group) are from Luo [68] and Liu et al. [69].

Table 9: The comparison of geological features between the Daping gold deposit and typical orogenic gold deposits.

Geological features	Typical orogenic gold deposits (Groves et al. [45]; Wang et al. [46]; Qiu et al. [60]; Xu et al. [1]; Lu et al. [61])	Daping gold deposit
Tectonic background	Tectonic compression environment of the orogenic belt	The Daping gold deposit is located in the transitional region of Xuefengshan orogenic belt between the Cathaysia plate and the Yangtze plate
Ore-bearing rocks	Most of the Archaean gold deposits occur in greenstone belts, and the ore-hosting rocks are mainly tholeiitic volcanic rocks. Phanerozoic gold deposits are mainly hosted in semideep sea or deep sea turbidite. The host rocks generally underwent shallow-medium metamorphism of greenschist facies and amphibolite facies	The wall rocks of the Daping gold ores are deep sea and semideep sea tuffaceous flysch formations of the Qingbaikou System with lithology assemblages mainly including slate, sandy slate, and sericite slate
Ore-controlling structure	The first-level fault is a large tectonic belt which cuts through the crust with a length of more than 100 km; the second-level fault has length of 1–10 km, and gold ore bodies are often located in the secondary level tectonic zones. The gold mineralization often occurred in the shear fracture and tension fracture	The Daping gold deposit is located in ca. 10 km southeast of the first-level deep fault of Anhua-Liping (about 350 km long). And second-level tectonics of the NE-trending ductile-brittle shear deformation zone of F8 (about 20 km long) cross through the Daping gold deposit from the middle. The mineralization structures are shear fracture of NW trend and tension fracture of the NE trend
Ore-type	The gold mainly occurred in the quartz veins with 3–5% metal sulfides	The gold mineralization mainly occurred in quartz veins and nearby metal sulfides, alteration rocks, and tectonic breccia rocks
Alteration type	K-feldspathization, silicification, sericitization, carbonization, and sulfidation	Silicification, sericitization, chloritization, carbonization, clayization, and sulfidation
Ore-forming fluids	Mantle-derived fluid, magmatic fluid, metamorphic fluid, and atmospheric water. The ore-forming fluids are characterized by CO_2-H_2O-NaCl±CH_4 and rich in CO_2	Magmatic fluid and atmospheric water. The ore-forming fluids are characterized by CO_2-H_2O-NaCl
Metallogenic temperature of the ore-forming fluids	150°C–700°C	157.3°C–255.8°C
Salinity of the ore-forming fluids	3–10 wt.% NaCl eqv.	4.57–10.93% (NaCl eqv.)
Assemblage of the metal elements	Au, Ag, ±As, Sb, Te, W, Bi	Au, As, ±Sb, ±Cu, ±Pb
Metallogenetic era	From the Neoarchaean to the Cenozoic era	The gold mineralization occurred in Indosinian era

vein with metal sulfides, the alteration of silicification and carbonization, and the ore-forming fluids of CO_2-H_2O-NaCl. In summary, the Daping gold deposit may belong to an orogenic type.

7. Conclusions

(1) The Daping gold ores have features of high content values of SiO_2, S, and As and low content values of Al_2O_3 and Na_2O and have intense alteration of silicification and sericitization. The gold ores are enriched in Li, Cr, Ni, Zn, Rb, Th, and Sr and depleted in Sc, Co, Cu, Ga, Cs, Tl, and Zr. The chondrite REE distribution patterns of the gold ores display strong enrichment of LREE with δEu values ranging from 0.54 to 0.75

(2) Four ore-forming stages were identified: the first stage has mineral assemblages of quartz+pyrite +arsenopyrite±carbonate minerals, the second stage has mineral assemblages of quartz+polymetallic sulfide minerals (pyrite, arsenopyrite, chalcocite, galena, chalcopyrite, tetrahedrite)±chlorite ±carbonate minerals, the third stage has mineral assemblages of quartz and carbonate minerals, and the supergene stage is characterized by limonite±patina which were formed by the oxidation of metal sulfides. Among them, the first stage and the second stage are the main gold mineralization stages

(3) The ore-forming fluid inclusions from quartz are composed of liquid phase (H_2O) and gas phase (H_2O and CO_2). The main gold mineralization stages of the first stage and second stage yielded average homogenization temperature of 184.5 and 255.8°C and average salinity of 7.64 wt.% NaCl eqv. and 11.35 wt.% NaCl eqv., respectively. Thus, the ore-forming fluids may belong to H_2O-CO_2-NaCl, medium-low temperature, and medium-low salinity fluids

(4) The values of $\delta^{34}S$ of metal sulfides in Daping gold deposit range from -0.94‰ to 1.98‰ (-0.131‰ in average), the δD_{H_2O} and $\delta^{18}O_{H_2O}$ values of auriferous quartz are from -51‰ to 62‰ and from -1.44‰ to 5.42‰, respectively, indicating that the sulfur may source from the concealed granite and/or Gaojian Group, and the ore-forming fluids may belong to mixing fluids of the magmatic fluid and meteoric hydrothermal fluid

(5) The Daping gold deposit formed in Indosinian period under the tectonic environment of compression between the Cathaysian plate and Yangtze plate and has similar features of the ore-bearing rocks, ore-controlling structures, alteration, and mineralization styles with typical orogenic gold deposits

Data Availability

The data used to support the findings of this study are included within the article.

Conflicts of Interest

The authors declare that they have no conflicts of commercial or associative interest with the submitted paper.

Authors' Contributions

Wentian Mi and Xu Kong equally contributed to the work; they are joint first authors.

Acknowledgments

This research was financially supported by the Open Research Fund Program of Key Laboratory of Metallogenic Prediction of Nonferrous Metals and Geological Environment Monitoring (Central South University), Ministry of Education (Grant no. 2017YSJS06), Open Research Fund Program of Geomathematics Key Laboratory (Chengdu University of Technology) of Sichuan Province (Grant no. scsxdz201602), Science & Technology Research Project of Department of Natural Resources of Hunan Province (Grant nos. 2017-02 and 2019-03), Natural Science Foundation of Inner Mongolia (Grant nos. 2019LH04002, 2020MS04009, and 2021MS04010), Key Laboratory of Geoscience Spatial Information Technology of Land and Resources of Chengdu University of Technology (Grant no. KLGSIT2016-02), and Scientific study project for institutes of higher learning of Ministry of Education of Inner Mongolia (Grant no. NJZZ19067). Special thanks are due to Dr. Wang Cheng for his valuable help in improving the quality of this paper and to my dearly beloved Xiang Li for her lasting vigorous support.

References

[1] D. R. Xu, T. Deng, G. X. Chi et al., "Gold mineralization in the Jiangnan Orogenic Belt of South China: geological, geochemical and geochronological characteristics, ore deposit-type and geodynamic setting," *Ore Geology Reviews*, vol. 88, pp. 565–618, 2017.

[2] D. Y. Bai, B. Li, C. Zhou et al., "Gold mineralization events of the Jiangnan Orogen in Hunan and their tectonic settings," *Acta Petrologica et Mineralogica*, 2021.

[3] J. L. Cao, "Genesis and occurrence characteristics of Au-bearing shear zone gold ore vein along with Xuefengshan Mountain range," *Hunan Geology*, vol. 20, no. 3, pp. 189–192, 2001.

[4] J. Z. Huang, J. Sun, C. Zhou et al., "Metallogenic regularity and resource potential of gold deposits of Hunan area in the Jiangnan Orogenic Belt, South China," *Acta Geoscientica Sinica*, vol. 41, no. 2, pp. 230–252, 2020.

[5] S. Y. Liu, Z. A. Bao, and J. M. Bao, "Gold deposit features and metallogenic regularity of Precambrian in Hunan province, China," *Geology and Mineral Resources of South China*, vol. 29, no. 1, pp. 37–45, 2013.

[6] X. G. Meng, Z. Y. Chen, Z. G. Shao, and X. Y. Feng, "Ore-controlling structures and genesis in the Tongxi gold field in the central segment of the Xuefeng Mountains," *Regional Geology of China*, vol. 20, no. 4, pp. 404–410, 2001.

[7] J. G. Zhao, L. Shu, H. H. Fu, and W. G. Song, "Study on technique of producing potassium aurocyanide," *Gold*, vol. 24, no. 5, pp. 8–12, 2003.

[8] D. G. Zhu, X. G. Meng, J. P. Wang, X. J. Tian, X. X. Liu, and J. G. Zhao, "Tectonic features of the major fractural zones and their control of minerogenesis in the gold area of the mid-Xuefengshan mountain, Hunan province," *Journal of Geomechanics*, vol. 4, no. 1, pp. 65–73, 1998.

[9] L. Cao, Q. F. Duan, S. G. Peng, and Y. Zhou, "Characteristics and geological significance of stable isotopes in the Chanziping gold deposit of Xuefeng Mountains," *Geology and Mineral Resources of South China*, vol. 31, no. 2, pp. 167–175, 2015.

[10] Y. J. Cao, J. Li, F. Chen, C. J. Wang, and B. D. Liu, "On geological characteristics and ore prospecting indicators of Chanziping gold deposit in Hunan," *Journal of Geology*, vol. 38, no. 2, pp. 309–313, 2014.

[11] X. Q. Luo, "Mineralization and prospecting guide of Chanziping gold deposit in Hunan," *Hunan Geology*, vol. 15, no. 1, pp. 33–38, 1996.

[12] S. J. LYU, S. S. Liu, Y. D. Li, and X. Kong, "Geological characteristics and genesis of Chanziping gold deposit in Xuefengshan area, Hunan Province," *Geology and Mineral Resources of South China*, vol. 35, no. 3, pp. 325–336, 2019.

[13] J. G. Zhao and Q. C. Chen, "Integrated prospecting model of ore characteristics, geophysics and geochemistry in the Chanziping gold deposit," *Land & Resources*, vol. 3, no. 3, pp. 80–83, 2006.

[14] Q. S. Zhou, *Detailed Report of the Daping Gold Deposit in Hongjiang City, Hunan Province*, No. 407 Geological Party of the Hunan Bureau of Geology and Mineral Exploration and Development, 2015.

[15] W. G. Tang, *General Report of the Daping Gold Deposit in Hongjiang City, Hunan Province*, No. 407 Geological Party of the Hunan Bureau of Geology and Mineral Exploration and Development, 1987.

[16] G. G. Fu, D. R. Xu, and K. M. Su, "Regularity of mineralization and ore-prospecting criteria of the Daping gold deposit, Hunan Province," *Journal of Earth Sciences and Environment*, vol. 32, no. S1, pp. 7-8, 2010.

[17] J. G. Zhao, "Geological characteristics of Au-deposit and its prospecting foreground at Daping gold mine, Hongjiang," *Hunan Geology*, vol. 20, no. 3, pp. 171–176, 2001.

[18] H. Q. Li, D. H. Wang, F. W. Chen, Y. P. Mei, and H. Cai, "Study on chronology of the Chanziping and Daping gold deposit in Xuefeng Mountains, Hunan Province," *Acta Geologica Sinica*, vol. 82, no. 7, pp. 900–905, 2008.

[19] C. Yang, *Analysis on ore-controlling structure and research on prospecting direction of gold-antimony in Xuefeng arc structure belt, [M.S. thesis]*, Hunan University of Science and Technology, 2012.

[20] X. G. Meng, D. G. Zhu, and X. X. Luo, *Analysis of ore-controlling structures and the evaluation of Au & Sb resources in the middle Xuefeng Mountain area*, Geological Publishing House, Beijing, 1999.

[21] K. M. Su, Z. Z. Xie, and W. G. Song, "Ore-controlling structures of gold deposits in the Xuefeng Mountain area," *Express Information of Mining Industry*, vol. 2006, no. 5, pp. 50–52, 2006.

[22] R. N. Clayton, J. R. O'Neil, and T. K. Mayeda, "Oxygen isotope exchange between quartz and water," *Journal of Geophysical Research*, vol. 77, no. 17, pp. 3057–3067, 1972.

[23] D. L. Hall, S. M. Sterner, and R. J. Bodnar, "Freezing point depression of NaCl-KCl-H_2O solutions," *Economic Geology*, vol. 83, no. 1, pp. 197–202, 1988.

[24] L. Y. Zhang, S. Y. Chen, and S. L. Liao, "Element and metallogenic significance of Jiufangliang gold deposit in Mianluening region, Shanxi Province," *Geological Science and Technology Information*, vol. 36, no. 2, pp. 151–159, 2017.

[25] C. Z. Xi, T. Yang, H. D. Xia, H. J. Deng, and S. G. Wu, "Characteristics of trace elements and REE in Huangjindong gold deposit in northeastern Hunan and their geological significance," *Gold*, vol. 39, no. 2, pp. 17–21, 2018.

[26] H. Ohmoto, "Systematics of sulfur and carbon isotopes in hydrothermal ore deposits," *Economic Geology*, vol. 67, no. 5, pp. 551–578, 1972.

[27] H. Ohmoto and R. O. Rye, "Isotopes of sulfur and carbon," in *Geochemistry of Hydrothermal Ore Deposits*, H. L. Barnes, Ed., pp. 509–567, Wiley, New York, 1979.

[28] L. Cao, Q. F. Duan, S. G. Peng, and Y. Zhou, "Characteristics of fluid inclusions in the Chanziping gold deposit in Xuefeng Mountain and their geological implications," *Geology and Exploration*, vol. 51, no. 2, pp. 213–224, 2015.

[29] Y. W. Han, Z. D. Ma, and H. F. Zhang, *Geochemistry*, vol. 2003, Geological Publishing House, Beijing, 2003.

[30] X. Kong, W. T. Mi, X. Mo, M. T. Xie, G. L. Jiang, and C. L. Fu, "Metallogenic prediction of gold deposits with weighting of evidence based on MRAS in Huaihua area, Hunan Province," *Geophysical and Geochemical Exploration*, vol. 40, no. 3, pp. 467–474, 2016.

[31] X. Kong, W. T. Mi, J. Xin, H. T. Chi, J. Hu, and Z. Y. Yang, "The gold metallogenic prognosis based on the weighting method of evidence in the middle Xuefeng Mountain area," *Computing Techniques for Geophysical and Geochemical Exploration*, vol. 41, no. 6, pp. 832–842, 2019.

[32] H. C. Niu, *Geochemical study on the minerogenetic background and mineralization of gold deposits in the Yiyang-Yuanling region of Hunan province, [Ph.D. thesis]*, Nanjing University, 1991.

[33] S. R. Taylor and S. M. McLennan, "The geochemical evolution of the continental crust," *Reviews of Geophysics*, vol. 33, no. 2, pp. 241–265, 1995.

[34] Q. K. Yang, X. L. Zhang, C. Hua, and P. Y. Xuan, "Geochemical characteristics of trace element of the molybdenite in the Dawangshan tungsten molybdenum polymetallic ore concentration area, Central Jiangxi Province," *Journal of Mineralogy and Petrology*, vol. 38, no. 2, pp. 59–69, 2018.

[35] J. H. Tao, T. Cen, W. G. Long, and W. X. Li, "Mineral chemistry of biotites from the Indosinian weakly peraluminous and strongly peraluminous granites in South China and their constraints on petrogenesis," *Earth Science Frontiers*, vol. 22, no. 2, pp. 64–78, 2015.

[36] D. Y. Bai, N. J. Wu, X. Zhong, P. Y. Jia, X. Xiong, and W. Y. Huang, "Geochronology, petrogenesis and tectonic setting of Indosinian Wawutang granites, southwestern Hunan province," *Geotectonica et Metallogenia*, vol. 40, no. 5, pp. 1075–1091, 2016.

[37] J. H. Li, Y. Q. Zhang, X. B. Xu, H. L. Li, S. W. Dong, and Y. D. Li, "SHRIMP U-Pb dating of zircons from the Baimashan-Longtan super-unit and Wawutang granites in Hunan province and its geological implication," *Journal of Jilin University: Earth Science Edition*, vol. 44, no. 1, pp. 158–175, 2014.

[38] H. Li, *Report of mineral geological survey in Longtan area, Hunan Province*, Internal information of Hunan Institute of Geology Survey, 2017.

[39] N. Y. Hu, Z. Y. Quan, L. Pan, and P. R. Wang, "Deformational characteristics of Xuefeng ARC structural belt and its relationship with Au-deposits," *Geotectonica et Metallogenia*, vol. 22, no. S1, pp. 33–37, 1998.

[40] D. K. Weatherley and R. W. Henley, "Flash vaporization during earthquakes evidenced by gold deposits," *Nature Geoscience*, vol. 6, no. 4, pp. 294–298, 2013.

[41] R. J. Goldfarb, D. I. Groves, and S. Gardoll, "Orogenic gold and geologic time: a global synthesis," *Ore Geology Review*, vol. 18, no. 1, pp. 1–75, 2011.

[42] F. Robert, R. Brommecker, B. T. Boume, P. J. Dobak, and X. Zhou, "Models and exploration methods for Major gold deposit types," *Ore Deposits and Exploration Technology*, pp. 691–711, 2007.

[43] J. W. Mao, G. Q. Xie, Z. H. Zhang et al., "Mesozoic large-scale metallogenic pluses in North China and corresponding geodynamic settings," *Acta Petrologica Sinica*, vol. 21, no. 1, pp. 169–188, 2005.

[44] M. Bonnemaison and E. Marcoux, "Auriferous mineralization in some shear zones: a three stage model of metallogenesis," *Mineralium Deposita*, vol. 25, no. 2, pp. 96–104, 1990.

[45] D. I. Groves, R. J. Goldfarb, M. Gebre-Mariam, S. G. Hagemann, and F. Robert, "Orogenic gold deposits: a proposed classification in the context of their crustal distribution and relationship to other gold deposit types," *Ore Geology Reviews*, vol. 13, no. 1-5, pp. 7–27, 1998.

[46] C. Wang, Y. J. Shao, N. J. Evans et al., "Genesis of Zixi gold deposit in Xuefengshan, Jiangnan Orogen (South China): age, geology and isotopic constraints," *Ore Geology Reviews*, vol. 117, article 103301, 2020.

[47] T. Deng, D. Xu, G. Chi et al., "Geology, geochronology, geochemistry and ore genesis of the Wangu gold deposit in northeastern Hunan Province, Jiangnan Orogen, South China," *Ore Geology Review*, vol. 88, pp. 619–637, 2017.

[48] C. Huang, G. M. Fan, G. L. Jiang, L. Luo, and Z. L. Xu, "Structural ore-controlling characteristics and electron spin resonance dating of the Yanlinsi gold deposit in northeastern Hunan Province," *Geotectonica et Metallogenia*, vol. 36, no. 1, pp. 76–84, 2012.

[49] J. W. Mao, R. Kerrich, H. Y. Li, and Y. H. Li, "High 3He/4He ratios in the Wangu gold deposit, Hunan province, China: implications for mantle fluids along the Tanlu deep fault zone," *Geochemical Journal*, vol. 36, no. 3, pp. 197–208, 2002.

[50] C. Wang, Y. J. Shao, X. Zhang et al., "Metallogenesis of the Hengjiangchong gold deposit in Jiangnan Orogen, South China," *Ore Geology Reviews*, vol. 118, article 103350, 2020.

[51] J. S. Wang, H. J. Wen, C. Li, W. Ding, and J. R. Zhang, "Re–Os isotope dating of arsenopyrite from the quartz vein-type gold deposit, southeastern Guizhou Province, and its geological implications," *Acta Geologica Sinica*, vol. 85, pp. 955–964, 2011.

[52] L. Zhang, L. Q. Yang, D. I. Groves et al., "Geological and isotopic constraints on ore genesis, Huangjindong gold deposit, Jiangnan Orogen, southern China," *Ore Geology Reviews*, vol. 99, pp. 264–281, 2018.

[53] D. Craw, S. J. Windle, and P. V. Angus, "Gold mineralization without quartz veins in a ductile–brittle shear zone, Macraes Mine, Otago Schist, New Zealand," *Mineralium Deposita*, vol. 34, no. 4, pp. 382–394, 1999.

[54] G. J. Davidson and R. R. Large, "Gold metallogeny and the copper-gold association of the Australian proterozoic," *Mineralium Deposita*, vol. 29, no. 3, pp. 208–223, 1994.

[55] B. N. Eisenlohr, D. Groves, and G. A. Partington, "Crustal-scale shear zones and their significance to Archaean gold mineralization in Western Australia," *Mineralium Deposita*, vol. 24, no. 1, pp. 1–8, 1989.

[56] J. L. Ni, J. L. Liu, X. L. Tang, C. Q. Zhao, and Q. D. Zeng, "Evolution of the ductile shear zone of the Paishanlou gold deposits, western Liaoning, China," *Science China: Earth Sciences*, vol. 57, no. 4, pp. 600–613, 2014.

[57] R. W. R. Rutland, M. A. Etheridge, and M. Solomon, "The stratigraphic and tectonic setting of the ore deposits of Australia," *Geology of the mineral deposits of Australia and Papua New Guinea*, vol. 14, pp. 15–26, 1990.

[58] Y. F. Zhu, J. Zhou, and Y. S. Zeng, "The Tianger (Bingdaban) shear zone hosted gold deposit, west Tianshan, NW China: petrographic and geochemical characteristics," *Ore Geology Reviews*, vol. 32, no. 1-2, pp. 337–365, 2007.

[59] No 407 Geol Team, *Periodic Report of Geological Prospecting Achievements of the Daping Gold Deposit in Hunan Province, China*, Hunan Bureau of Geology and Mineral Exploration and Development, 2015.

[60] Z. J. Qiu, H. R. Fan, P. Z. Cong, X. Liu, and K. F. Yang, "Recent progress in the study of ore-forming processes of orogenic gold deposits," *Mineral Deposits*, vol. 34, no. 1, pp. 21–28, 2015.

[61] H. Z. Lu, G. X. Chi, X. Q. Zhu, J. Guha, G. Archambault, and Z. G. Wang, "Geological characteristics and ore forming fluids of orogenic gold deposits," *Geotectonica et Metallogenia*, vol. 42, no. 2, pp. 244–265, 2018.

[62] S. S. Sun and W. F. McDonough, "Chemical and isotope systematics of oceanic basalts: implications for mantle composition and processes," in *Magmatism in Ocean Basins*, A. D. Saunders, Ed., vol. 42, pp. 313–345, Geological Society Publication, 1989.

[63] W. V. Boynton, "Cosmochemistry of the rare earth elements: meteorite studies," in *Rare Earth Element Geochemistry. Amsterdam*, pp. 64–114, Elsevier, 1984.

[64] H. P. Taylor, "Oxygen and hydrogen isotope relationships in hydrothermal mineral deposits," *Geochemistry of Hydrothermal Ore Deposits*, vol. 3, pp. 229–302, 1997.

[65] J. Y. Luo, *Genetic mineralogy and ore prediction of Yixingzhai gold deposit, Fanshi County, Shanxi Province*, vol. 2009, Dissertation of China University of Geosciences (Beijing) for doctoral degree, 2009.

[66] N. X. Peng, Y. J. Shao, Z. F. Liu, and C. Wang, "Metallogenic mechanism of Yixingzhai gold ore field in Fanshi county, Shanxi province: evidences from isotopes and fluid inclusion," *The Chinese Journal of Nonferrous Metals*, vol. 27, no. 2, pp. 305–317, 2017.

[67] C. Wang, Y. Shao, Z. Liu, Q. Liu, and Y. Zhang, "Geology and geochemistry of the Shizitou molybdenum deposit, Jiangxi Province: implications for geodynamic setting and metallogenesis," *Acta Geologica Sinica (English Edition)*, vol. 92, no. 4, pp. 1415–1431, 2018.

[68] X. Luo, "Discussion on the material sources of gold deposits in Precambrian strata in Hunan," *Journal of Guilin Institute of Metallogenic Geology*, vol. 10, pp. 13–25, 1990.

[69] L. Liu, S. Peng, and Y. Wu, "Genetic features forming vein type gold deposits in northeastern Hunan," *Journal of Central South University of Technology (Natural Science)*, vol. 30, pp. 4–7, 1999.